Theor Chem Acc (2011) 130:455–462
DOI 10.1007/s00214-011-1023-8

REGULAR ARTICLE

High-pressure transitions in bulk mercury: a density functional study

S. Biering · P. Schwerdtfeger

Received: 29 March 2011 / Accepted: 13 August 2011 / Published online: 21 September 2011

Abstract We provide a consistent treatment of the known solid-state phases of mercury to high pressure to determine the phase changes at 0 K by using the local density approximation (LDA). We obtain good agreement with experimental measurements demonstrating that LDA performs well in the repulsive region of the inter-atomic interaction. The known α-, β-, γ-, and δ-phases of mercury differ energetically by no more than 0.04 eV and therefore provide a challenge to future high accuracy calculations using either wavefunction or density functional-based approximations.

Keywords Mercury · Hg · High pressure · Solid state · Structure · Density functional theory

1 Introduction

Mercury is an extraordinary element with many unique properties that are still not fully understood [1]. With an exceptionally low melting temperature of 234.3 K [2] it is the only liquid metal at room temperature with a very broad temperature range for the liquid state compared to other metals [3]. Only very few other metals solidify at rather low temperature, those are cesium, francium, gallium, and rubidium. The low melting temperature of mercury is assumed to be of relativistic origin [4], i.e., a consequence of the very strong relativistic 6*s* orbital contraction/stabilization, which substantially influences the chemistry and physics of mercury [1] leading often to surprising results [5–7]. Here, we mention that the high superconducting transition temperature of Hg (4.15 K) in contrast to Zn (0.85 K) or Cd (0.52 K) [8] has been suggested to be of relativistic origin [9] (see also the discussion in ref. [10]). Furthermore, it has been observed that electronic properties, in particular, the electrical conductivity, of liquid mercury are special as they are strongly dependent on the density of the liquid [11].

In its solid state, mercury is equally interesting, as an early investigation by McKeehan and Cioffi [12] determined a rhombohedral structure at -115°C with a lattice constant of $a = 3.025$ Å and a rhombohedral angle of $\alpha = 70°31.7'$, as shown in Fig. 1. This so-called α-phase (space group $R\bar{3}m$ or 166) was the first simple rhombohedral arrangement observed for an elementary substance and has even now only been found as a high-pressure phase of lithium [13]. The question was raised whether a closer packing (hcp) could be possible, similarly to what is found for other members of the same group such as Zn, Cd, and Mg [14]. The origin of the unusual solid-state structure of mercury has been investigated extensively using theoretical methods by Singh, Paulus, Gaston, and others and could be explained by a subtle interplay between relativistic effects and the influence of electron correlation [15–19].

Dedicated to Professor Shigeru Nagase on the occasion of his 65th birthday and published as part of the Nagase Festschrift Issue.

S. Biering · P. Schwerdtfeger (✉)
Centre for Theoretical Chemistry and Physics,
The New Zealand Institute for Advanced Study,
Massey University Albany, Private Bag 102904,
North Shore MSC, Auckland 0745, New Zealand
e-mail: p.a.schwerdtfeger@massey.ac.nz

S. Biering
e-mail: s.b.biering@massey.ac.nz

P. Schwerdtfeger
Fachbereich Chemie, Philipps-Universität Marburg,
Hans-Meerwein-Str., 35032 Marburg, Germany

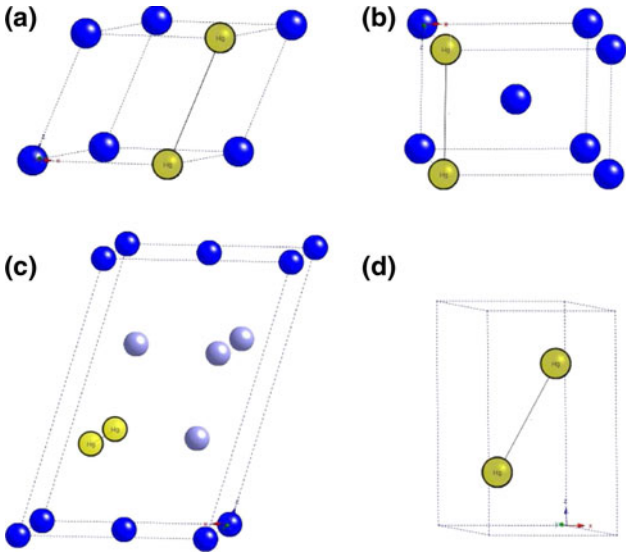

Fig. 1 Crystal structures for the different phases of mercury: **a** α-Hg, rhombohedral; **b** *β*-Hg, *I4/mmm*; **c** *γ*-Hg, *C2/m*; **d** *δ*-Hg, hcp. *Dark blue colored* atoms represent sites with multiplicity 1*a*, 2*a* or 2*c*; *light blue* sites with multiplicity 4*i*. *Yellow labeled* atoms indicate the closest Hg–Hg bond

The high-pressure behavior of mercury is not less intriguing since it gives rise to quite unique crystal structures as well, as shown in Fig. 1. Experimental studies have revealed that, if investigated at room temperature, at approximately 1.2 GPa liquid mercury solidifies into the rhombohedral α-Hg structure. A transformation into the *β*-phase is observed at 3.4 GPa [20]. It has a body-centred tetragonal structure with space-group *I4/mmm* (139). This rearranges into the *γ*-Hg phase at 12 GPa [21, 22], for which Schulte and Holzapfel first suggested an orthorhombic arrangement. However, using angle-dispersive powder X-ray diffraction, Takemura et al. [20] obtained a monoclinic crystal structure with six atoms in the unit cell (space group *C*2/*m* or 12). The atoms are placed at the 2*a* (0, 0, 0) and 4*i* (*x*, 0, *z*) positions. Takemura et al. [20] specifically emphasize a need for further theoretical investigations of the *γ*-phase to confirm its stability. Finally, the *γ*-phase transforms into the hexagonal close-packed (hcp) structure at high pressure of 37 GPa [21] that remains stable up to at least 193 GPa [20], or perhaps even 1 TPa according to first-principles calculations [23]. It is known as *δ*-Hg (*P*6$_3$/*mmc* or 194), and the structure has a rather large *c*/*a*-ratio, similarly to the respective phase in Zn and Cd. This leads to the following transition path: α-Hg $\overset{3.4\text{GPa}}{\longrightarrow}$ *β*-Hg $\overset{12\text{GPa}}{\longrightarrow}$ *γ*-Hg $\overset{37\text{GPa}}{\longrightarrow}$ *δ*-Hg. The corresponding phase diagram is shown in Fig. 2.

While those phases are frequently studied experimentally, little effort has been put into computational investigations (except for α- and *δ*-Hg [15–19, 24]). Interesting is especially the transition under extremely high pressure into

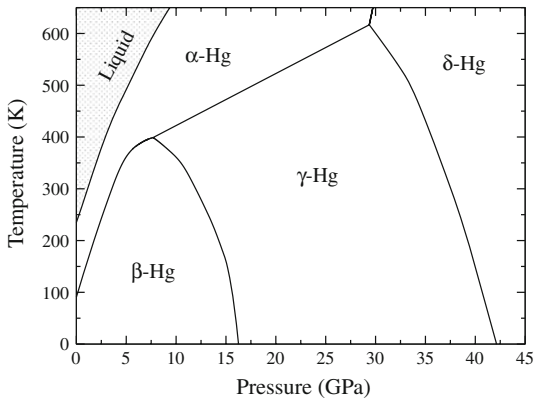

Fig. 2 Pressure–temperature phase diagram of mercury obtained from data in ref. [22]

the close-packed system. In addition to the observed hcp phase, a close-packed face-centred cubic arrangement could also be possible. Here, we note that large differences between hcp and fcc structures originate from large contributions from three- and higher body forces or even quantum fluctuations, as simple two-body interactions give only small energy differences between the two closed-packed structures [25, 26]. Theoretical studies of those two structures in comparison with the experimentally observed arrangements could shed some light on the question, why for mercury hcp is favored over the fcc structure. Hence, we decided to perform local density functional calculations for the different known phases of solid mercury, which might raise interest in future investigations using more elaborate and accurate wavefunction and density functional-based approximations. We note that it still remains a major challenge to modern quantum chemistry to successfully model the phase transitions at various temperatures and pressures by first principle methods.

2 Computational methods

Periodic calculations based on density functional theory by means of the localized density approximation (LDA) [27] in conjunction with a plane-wave basis set as implemented in the Vienna Ab-initio Simulation Package VASP [28, 29] were performed. Note that the LDA was found to give good results for metallic mercury in the overlap region, while other gradient corrected density functionals failed and led to weak or even no binding for the solid phase [30]. It was pointed out recently that the binding in solid mercury is purely an electron correlation effect [17], and adding exact exchange to the density functional has, therefore, a destabilizing effect [30]. Nevertheless, we briefly discuss the performance of other functionals as well, i.e., PW91 according to Perdew and Wang [31, 32], PBE by Perdew,

Burke and Ernzerhof [33], as well as the revised PBE functional for solids (PBEsol) [34]. In addition, the DFT-D2 method of Grimme has been employed in conjunction with the global scaling parameter s_6 as optimized for PBE ($s_6 = 0.75$) [35, 36], abbreviated as PBE-D in the following.

The projector augmented-wave (PAW) method including scalar relativistic effects in the valence space from the pseudopotential approximation [29, 37–39] was employed to describe the interaction of the atomic core region with the explicitly treated (outermost 5*d* plus 6*s*) valence electrons. This allows to reduce the number of plane waves per atom to a minimum while achieving a high accuracy treatment of the Hg-5*d* electrons. After carefully checking for convergence, plane waves with kinetic energies of up to 29.4 Ry were included. The integrations over the Brillouin zone for the calculation of the electronic densities and total energies are substituted by summations over a specially weighted uniform Monkhorst-Pack type [40] *k*-point mesh that includes the Γ-point and was thoroughly tested to assure converged results.

For the determination of the equilibrium properties (unless otherwise stated), a full geometry optimization was carried out for the different crystal structures, while keeping the unit-cell volume constant. By those means, the cell shape as well as the internal parameters were allowed to relax for a band of fixed unit-cell volumes and the according total energy calculated. The obtained energy–volume dependencies were then fitted to the Murnaghan equation of state [41], which immediately gives the equilibrium volume V_0, the total energy per atom E_0 at zero K, the zero-pressure bulk modulus B_0 as well as its pressure derivative $B' = dB/dp$. From the total energy per atom E_0, the cohesive energy (atomization) was calculated by subtracting the total atomic energy. The latter was determined beforehand in single atom calculations in a carefully converged box size, where the plane-wave cutoff was chosen to be equivalent to the one used for the crystal structure optimization.

Since our calculations are limited to low temperatures and neglect phonon contributions, the in fact suitable thermodynamic potential, the Gibbs free energy $G = U + pV - TS$, can be approximated by the enthalpy of the system $H = E + pV$ ($U(V) \approx E(V)$). Hence, the transition pressures are predicted from the crossing of two graphs of different structures in the $H(p)$-plot. The zero-point energy is neglected which is estimated to be 0.01 eV [18].

3 Results and discussion

The calculated energy–volume dependencies for the according crystallographic phases of bulk mercury using LDA are depicted in Fig. 3. The experimentally observed

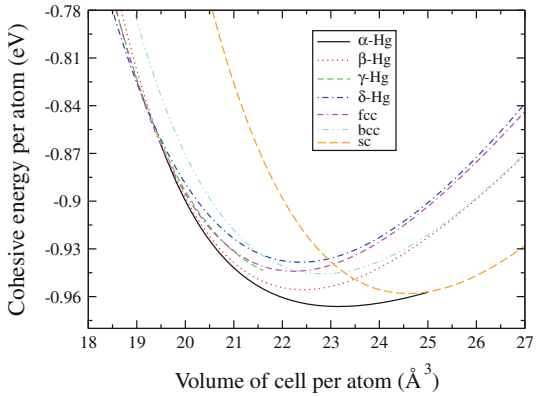

Fig. 3 Cohesive energy versus volume per atom for different crystal structures of bulk mercury from LDA calculations

trend with increasing pressure is confirmed. We find a ground-state volume of 23.14 Å^3 for the rhombohedral α-phase in good agreement with other theoretical and experimental work (see Table 1). While the lattice parameter of 2.947 Å compares well to the experimentally observed values (e.g., 2.986 Å at 5 K [42]), this is not the case for the rhombohedral angle. It is calculated to be 74.21°, overestimating the actual value of 70.74° (at 5 K) [42]. However, the potential energy surface is rather shallow along the rhombohedral angle as pointed out before by Gaston et al. [18]. As expected, the LDA cohesive energy of 0.966 eV is overestimated compared to the experimentally estimated value of 0.67 eV [47]). As mentioned before, this weak performance of density functional theory has been the subject of an intensive study by Gaston et al. [18, 19], who found even larger discrepancies (not only for the cohesive energy, but even for the crystallographic parameters) for PBE, PW91, PB86, and B3LYP (see also Table 1), and LDA has been found to be still the most reliable functional for mercury in its solid state. However, a significant improvement of the results could be achieved using an explicit treatment of electron correlation in terms of the incremental method [43] or the random-phase approximation recently implemented by Harl and Kresse or Scuseria and co-workers [44–46], which are, however, very computer time intensive. For the bulk modulus, a value of 25.9 GPa along with a pressure constant of 11.1 is determined using the full geometry optimization. This is in acceptable agreement with experimental results as can be read from Table 1, and similar values have been obtained in other theoretical studies. As expected, the bulk modulus obtained from the incremental method by Gaston and coworkers [18] again seems to be much more reliable.

To further investigate the nature of the α-Hg phase, the rhombohedral structure can be considered as a rhombohedral distortion of the fcc lattice. The primitive unit vectors can then be expressed as $\vec{a}_1 = a'(1+x, x, x)$, $\vec{a}_2 =$

Table 1 Ground-state properties of different mercury phases

Property	This work	Other theoretical	Experiments
α-Hg			
a	2.947	2.971/3.894/3.535/3.540[a], 2.96[b]	2.986/2.993[d], 3.005[e]
α	74.21	72.6/89.5/61.2/60.9[a], 69.5[b]	70.74[d], 70.53[e]
V_0	23.14	23.23/59.04/32.08/32.00[a], 21.97[b], 23.04[c]	22.99/23.15[d], 23.35[e]
B_0	25.9	18.7[a], 36.0[b], 67.6[c],	38.2[c], 32.2[f]
B'	11.1		
E_{coh}	−0.966	−0.918/−0.044/−0.195/−0.164[a], −0.649[b]	−0.67[e]
p_t to β	6.5		3.7[g,h], 3.4[i]
β-Hg			
a	4.022 (3.714)		(3.688)[i], 3.995[k]
c	2.793 (2.785)		(2.800)[i], 2.825[k]
c/a	0.694 (0.750)		(0.759)[i], 0.706[k]
V_0	22.60 (19.21)		(20.8)[g], 24.0[h], (19.04)[i], 22.54[k]
B_0	52.3		(81)[g], 35[h]
B'	4.2		(2)[g], 7.0[h]
E_{coh}	−0.957		
p_t to γ	9.3		12[g,h]
γ-Hg			
a	(5.192)		(2.691)[g], (5.179)[i]
b	(2.826)		(4.457)[g], (2.797)[i]
c	(7.849)		(6.454)[g], (7.964)[i]
β	(108.18)		(107.96)[i]
b/a	(0.544)		(0.540)[i]
c/a	(1.512)		(1.538)[i]
x	(0.770)		(0.762)[i]
z	(0.335)		(0.333)[i]
V_0	22.21 (18.25)		(18.7)[g], 23.9[h], (18.29)[i]
B_0	60.3		(267)[g], 22[h]
B'	5.3		(8.5)[g], 13.5[h]
E_{coh}	−0.946		
p_t to δ	35.6		37[g], 35–43[i]
δ-Hg			
a	3.067 (2.810)	3.06[a], 3.58[j], (∼2.9)[k]	(2.815)[i],
c	5.493 (4.866)	(∼5.0)[k]	(4.927)[i],
c/a	1.791 (1.732)	(∼1.7)[k]	(1.750)[i]
V_0	22.37 (16.64)	(∼17.5)[k]	(16.14)[g], 22.5[h], (16.91)[i]
B_0	49.1	19[a], 21[j]	(271)[g], 78[h]
B'	5.6		(4.2)[g], 4.2[h]
E_{coh}	−0.938	−0.813[a]	

Presented are the lattice constants a, b, and c (Å), angles α and β, respective internal parameters, ground-state volume V_0 (Å^3/atom), bulk modulus B_0 (GPa) and its pressure derivative B' as well as the cohesive energy E_{coh} (eV) and the transition pressure p_t (GPa) where applicable. Values in brackets indicate a higher pressure above the transition (see legend of references below), i.e., 15.0, 20.9, and 40.5 GPa for β-, γ-, and δ-Hg, respectively, for this work

[a] LDA/B3LYP/PW91/PBE DFT from ref. [18]

[b] Incremental electron correlation (up to 3-body terms) from ref. [18]

[c] GTP-LDA from ref. [23] and refs. therein

[d] X-ray powder diffraction (XRD) at 1 Pa and 5 K/78 K from ref. [42]

[e] At 225.15 K from ref. [47]

[f] From ref. [48]

[g] Energy-dispersive X-ray diffraction (EDXD) at 8 (β-Hg), 27 (γ-Hg) and 40 GPa (δ-Hg) from ref. [21]

[h] EDXD from ref. [22]

[i] XRD from ref. [20] at 20 (γ-Hg) and 35.2 GPa (δ-Hg) and refs. therein (at 15 GPa for β-Hg)

[j] LMTO from ref. [16]

[k] FPLAPW-GGA at 0 K and ∼40 GPa from ref. [24] and refs. therein (at 77 K)

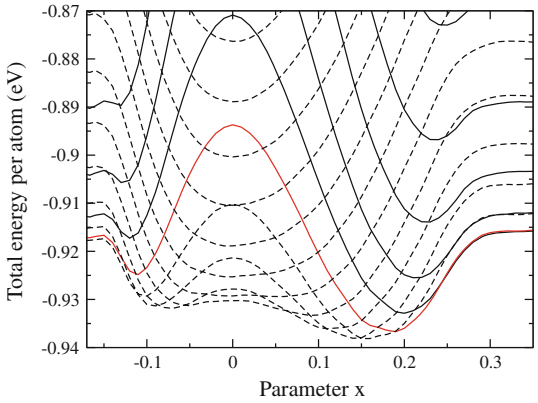

Fig. 4 Variation of the total energy with respect the rhombohedral distortion x. The *red graph* shows the optimized volume (with respect to experimental results) for the α-Hg structures, whereas the *black solid* and *dashed lines* indicate curves of lower and higher volumes (in steps of 0.5 Å^3), respectively

$a'(x, 1+x, x)$, $\overrightarrow{a}_3 = a'(x, x, 1+x)$, where the parameter x is a qualitative measure of the grade of distortion. Hence, $x = 1/3$ ($\alpha = 60°$) equals the fcc structure. Similarly, this description also immediately yields the bcc and sc structures for $x = -1/6$ ($\alpha = 109.5°$) and $x = 0$ ($\alpha = 90°$), respectively (see Table 3 for the ground-state properties of the cubic structures). This way it is possible to map the total energy depending on the volume V of the unit cell and the parameter x, where the experimentally observed value for the rhombohedral angle is equivalent to $x = 0.19$. The resulting potential energy curves with varying parameter x for different volumina are shown in Fig. 4, with a two-dimensional view of the total energy versus volume in Fig. 5. Only for the red curve in Fig. 4, equivalent to a unit-cell volume of 22.5 Å^3, lattice parameters of $\alpha = 70.8°$ and $a = 2.964$ Å can be obtained, closely resembling the experimental results. Furthermore, this curve compares well to early theoretical investigations by Weaire [49] and Moriarty [23]. However, toward higher volumes (dashed lines), the minimum slowly converges to $x = 0$. Hence, for negative pressures, the rhombohedral phase of mercury becomes identical to the simple cubic structure, see also Fig. 3. On the other hand, with increasing pressures (solid lines), the minimum quickly moves toward the fcc structure ($x = 1/3$). This is in disagreement with previous work [18], where a simple cubic structure at small bond distances, and fcc at larger bond distances was obtained (NB: these published curves were not fully optimized $E(V)$ curves and obtained with small Gaussian basis sets). The second lowest minimum, found around $x = -0.1$ ($\alpha \approx 50°$), can be interpreted as γ-Hg, indicating a distortion of the fcc lattice in opposite direction of α-Hg according to ref. [23].

To discuss the validity for our choice to apply the LDA, the potential energy surface with respect to the

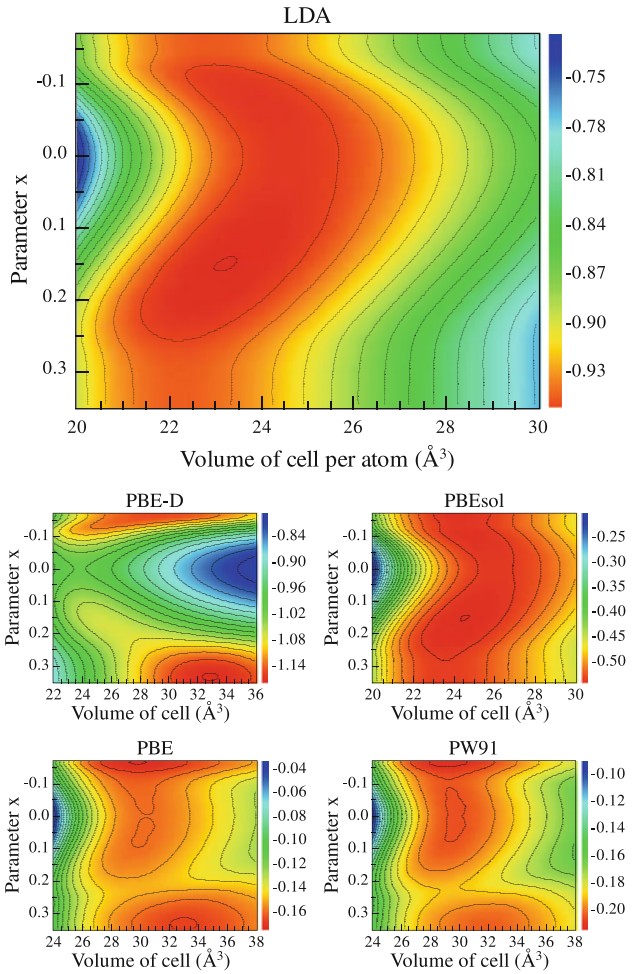

Fig. 5 Potential energy surface plotted with respect to the unit-cell volume per atom as well as the rhombohedral distortion x for a variety of density functionals. The *color bar* down the *right-hand side* indicates the cohesive energy per atom in eV. The energy difference between *contour lines* is 25 (PBE-D), 15 (LDA and PBEsol), and 7.5 meV (PBE and PW91), respectively. The obtained structure is equal to the bcc, sc, and fcc lattice if $x = -1/6$, 0, and 1/3, respectively

rhombohedral distortion x and the unit-cell volume V have also been calculated using the generalized gradient approximation (GGA) [50], i.e., PW91 [31, 32], PBE [33], PBEsol [34], and PBE-D [35, 36]. The results are also shown in Fig. 5 and clearly confirm that none of the investigated functionals perform as well as LDA. The standard functionals PBE and PW91 predict fcc and sc, respectively, to be more stable than the α-Hg structure as also shown by Table 2. The obtained cohesive energies and ground-state volumes are in excellent agreement with a study by Gaston et al. [18] (see Table 1), even though the respective authors calculate fcc as the ground-state structure for both functionals. However, it should be acknowledged that the differences in cohesive energy, in particular, for PW91, are very small. In general, both functionals severely underestimate the cohesive energies while

Table 2 Comparison of the ground-state properties of the α, fcc, and sc mercury phases calculated using different density functionals

Functional	α-Hg		fcc		sc	
	E_{coh}	V_0	E_{coh}	V_0	E_{coh}	V_0
PBE-D	−1.067	26.77	−1.175	32.95	−1.001	23.81
PBEsol	−0.551	24.22	−0.536	23.58	−0.540	26.03
PBE	−0.160	30.18	−0.167	33.12	−0.159	30.43
PW91	−0.204	28.99	−0.203	31.73	−0.205	29.78

Presented are the ground-state volume V_0 (Å^3/atom) and the cohesive energy E_{coh} (eV). See Table 1 to compare to other theoretical results

overestimating the ground-state volume. Surprisingly, the dispersion corrected PBE-D functional performs just as bad, strongly favouring the fcc arrangement over the α-Hg structure. However, the calculated energies are more reasonable than with PBE or PW91. On the other hand, PBEsol gives very good results for the optimized geometry, being the only functional that also correctly predicts α-Hg to be the preferred structure. The calculated ground-state volume of 24.22 Å^3/atom and the lattice constant $a = 3.023$ Å is in rather good agreement with experimental results. Comparison is even better for the rhombohedral angle $\alpha = 71.85°$ (see Table 1 for experimental values). With respect to the predicted structure, PBEsol, hence, performs even better than LDA. Yet, the functional fails to predict the correct cohesive energy, which makes it unsuitable for the determination of transition pressures to investigate the high-pressure behavior of solid mercury. We mention that for the PBE, GGA, and PBE-D calculations, the ground-state properties for the α-Hg phase may not be as accurate as the results for LDA and PBEsol. This is due to the fact that, for those functionals, with increasing volumes, the α-Hg phase becomes too unstable with respect to the fcc or sc arrangement (depending on the according functional). Since the structure optimization is carried out under the constraint of keeping the volume constant, the respective rhombohedral angle, therefore, simply converges to 60 or 90°, respectively. Hence, the ground-state properties for the α-Hg phase were obtained by fitting the Murnaghan equation of state to only the data points that converged to the actual α-Hg structure.

Generally, the question remains why we should predict α-Hg as the equilibrium phase of mercury. At low temperatures and low pressures, mercury is known to crystallize in the β-Hg structure according to the phase diagram derived by Schulte and Holzapfel [22] (see Fig. 2). These authors assume the values for the $\alpha - \beta$ transition mainly from ref. [51]. However, they observed the transition only down to a value of 1 kbar at which the transition occurs at approximately 98 K. The slope could well be steeper at lower pressures adding uncertainty to the relative stability of both phases. In addition, an experimental study by Barrett [42] investigates the rhombohedral α-phase down to a temperature of 5 K. Nevertheless, from the theoretical point of view, the energy difference between both structures is only 0.02 eV at the LDA level of theory. The zero-point energy difference between both structures is expected to be of a few meV (from the Debye temperature of mercury or from cluster extrapolations [30], we obtain a zero-point vibrational energy between 0.008 and 0.01 eV for solid mercury [19]). Yet, keeping this in mind, we predict that the α-Hg phase transforms into β-Hg at approximately 6.5 GPa. This is in perhaps fortuitous good agreement with the experimental findings of Schulte and Holzapfel who observe the transition at 3.7 GPa (obtained, however, at room temperature) [21, 22]. However, a correct treatment of this phase transition requires more sophisticated methods and the inclusion of thermal effects.

For the β-phase of mercury, we calculate a ground-state volume of 22.60 Å^3 per atom along with a cohesive energy of −0.957 eV. Both parameters are very close to the rhombohedral arrangement. The corresponding values for the lattice parameters are $a = 4.022$ Å and $c = 2.793$ Å ($c/a = 0.694$), in very good agreement with the experimental results (see Table 1). The bulk modulus of 52.3 GPa and its pressure derivative (4.2), however, deviate strongly from experiment, which is rather common in DFT calculations in general. Moreover, finite temperature effects, which we neglect, are important for the bulk modulus. Unfortunately, no other theoretical work could be found to compare to. At a pressure of 15.0 GPa above the calculated transition pressure, but at a comparable value to ref. [20], we obtain $V = 19.21$ Å^3, $a = 3.714$ Å, $c = 2.785$ Å ($c/a = 0.750$), in excellent agreement with their work.

At approximately 9.3 GPa, the β-Hg phase transforms into the γ-Hg structure. This is again in good agreement with experimental results ($p_t = 12$ GPa [21]). Even though Schulte and Holzapfel [22] suggested an orthorhombic arrangement for this phase, the structure could not be clearly resolved, and hence, the newly suggested monoclinic structure [20] has been investigated here. For this monoclinic structure, the estimated ground-state volume of $V_0 = 22.21$ Å^3/atom at zero pressure agrees with the experimental data (see Table 1). However, with increasing volume, the γ-Hg structure seems to become energetically less stable and it was not possible to get converged results for this crystallographic arrangement above a volume of $V = 21.6$ Å^3 per atom. The given ground-state volume, bulk modulus ($B_0 = 60.3$ GPa), and its pressure derivative ($B' = 5.3$) are therefore predicted only from the fit of the Murnaghan EOS to the points available and hence deviate rather strongly from the experimental data available. Consequently, it was also not possible to obtain results for the lattice constants and the internal parameters at 0 Pa.

However, at a pressure of 20.9 GPa above the transition, the ground-state volume and lattice parameters are as follows: $a = 5.192$ Å, $b = 2.826$ Å, $c = 7.849$ Å, $b/a = 0.544$, $c/a = 1.512$, and $V = 18.25$ Å^3. The Wyckoff parameters are $x = 0.770$ and $y = 0.335$. Those values compare very well to experiment, in particular, if one considers the large number of the degrees freedom for this crystallographic structure. Moreover, the values are in excellent agreement with results of Takemura and coworkers (see Table 1). Hence, we conclude that indeed the monoclinic $C2/m$ structure should be considered as the high-pressure γ-phase for mercury. Furthermore, it is mentioned that the energy difference between the α- and the proposed γ-phase in the calculation of Moriarty [23] as estimated from the figures is 0.025 eV. This is comparable to the value obtained here ($\Delta E_{\mathrm{coh}}(\gamma - \alpha) = 0.020$ eV).

At higher pressures, the lattice parameters slowly converge toward the close-packed hexagonal structure and at 35.6 GPa the transformation into the δ-Hg phase is finally achieved. Takemura et al. suggest the coexistence of the γ- and the δ-phase between 35–43 GPa [20] and another study observes hexagonal mercury from 30 GPa onwards (at room temperature) [21]. The ground-state volume of the hcp phase is calculated to be 22.37 Å^3 per atom, which compares very well to an estimate given by ref. [22] ($V_0 = 22.5$ Å^3/atom). Our bulk modulus of 49.1 GPa is, however, severely underestimated compared to experiment ($B = 78$ GPa [22]), but somehow better than in other theoretical work [16, 19]. Moreover, the cohesive energy is not very well described by LDA if compared to the incremental result by Gaston et al. (−0.813 eV [19]). Looking at the properties at significantly higher pressures above the transition (40.5 GPa), the values derived for the lattice constants ($a = 2.810$ Å, $c = 4.866$ Å, $c/a = 1.732$) are in excellent concordance with the experiment by Takemura [20] (see Table 1), as is the unit-cell volume. Furthermore, the behavior of the lattice parameters and unit-cell volume with increasing pressure agree very well with a recent theoretical study [24]. The author's results at around 40 GPa are estimated from their graphs and can be seen in Table 1. The rather high c/a-ratio is confirmed as well.

It should be mentioned that according to our calculations, the fcc structure is extremely close to β- and γ-Hg in the transition region between the two phases, Fig. 3. This can also be gathered from the extremely similar ground-state properties of γ-Hg and the fcc arrangement (compare Tables 1, 3), suggesting a rather small distortion of the γ-phase with respect to the fcc structure. The respective transition pressure for the hypothetical β-Hg to fcc transition is 12.2 GPa. Hence, from a theoretical point of view, a fcc high pressure form of mercury cannot be ruled out. In contrast, the bcc arrangement is rather high in energy compared to all other structures and therefore can be disregarded as a high-pressure phase for mercury. This is also evident from the rather large nearest neighbor distance compared to the other structures as shown in Table 4.

Table 3 Ground-state properties of hypothetical mercury phases

System	E_{coh}	V_0	B_0	B'	a
fcc Ref. [16]	−0.944	22.23	51.7	7.6	4.463
		31.82	48		5.03
bcc	−0.946	22.83	47.8	6.7	3.574
sc	−0.958	24.59	51.7	7.0	2.908

Presented are the lattice constants a (Å), ground-state volume V_0 (Å^3/atom), bulk modulus B_0 (GPa), and its pressure derivative B' as well as the cohesive energy E_{coh} (eV)

Table 4 Summary of closest Hg–Hg distance d_{nn} in Å and number of nearest neighbors X_{nn} for several mercury phases

System	d_{nn}	X_{nn}	System	d_{nn}	X_{nn}
α	2.95	6	fcc	3.16	12
β	2.79 (2.79)	2	bcc	3.57	8
γ	(2.76)	2	sc	2.91	6
δ	3.07 (2.81)	6			

Values in brackets indicate a higher pressure above the phase transition, i.e., 15.0, 20.9 and 40.5 GPa for β-, γ- and δ-Hg, respectively

4 Summary and conclusion

In a first attempt, we tried to describe pressure-induced phase transitions in solid mercury at the zero Kelvin line using LDA. The results clearly show that there are many open questions, and the phase diagram for solid mercury is to our opinion still not well understood, especially at very low temperatures. More experimental and accurate theoretical studies (including spin-orbit effects) are required for a complete description of mercury in the solid state. Hence, the accurate description of mercury from the dimer [52] to clusters [30] and finally the solid and liquid phase remains an unresolved challenge to electronic structure theory.

Acknowledgments We gratefully acknowledge the financial support by the Royal Society of New Zealand in terms of the Marsden grant (MAU0703). PS is indebted to the Alexander von Humboldt Foundation (Bonn) for financial support during the stay in Marburg. Finally, we thank Prof. Friedrich Hensel (Marburg) and Dr. C. Thierfelder (Paderborn) for helpful discussions.

References

1. Pahl E, Schwerdtfeger P (2010) In: Sattler KD (ed) Handbook of nano-physics, vol 2, Chap. 3. Taylor and Francis, London, pp 1–13
2. Hill KD (1994) Metrologia 31:39

3. Hensel F, Warren WW Jr (1999) Fluid metals. Princeton University Press, Princeton
4. Pyykkö P (1988) Chem Rev 88:563
5. Höltzl T, Nguyen MT, Veszprémi T (2010) Phys Chem Chem Phys 12:556
6. Wang X, Andrews L, Riedel S, Kaupp M (2007) Angew Chem Int Ed 46:8371
7. Zaleski-Ejgierd P, Pyykkö P (2009) J Phys Chem A 113:12380
8. Matsubara T (1982) The structure and properties of matter. Springer, Heidelberg
9. Schwerdtfeger P, Dolg M, Schwarz WHE, Bowmaker GA, Boyd PDW (1989) J Chem Phys 91:1762
10. Deng S, Simon A, Köhler J (1998) Angew Chem Int Ed 37:640
11. Mattheiss LF , Warren WW Jr (1977) Phys Rev B 16:624
12. McKeehan LW, Cioffi PP (1922) Phys Rev 19:444
13. Hanfland M, Syassen K, Christensen NE, Novikov DL (2000) Nature 408:174
14. Donohue J (1974) The structures of the elements. Wiley, New York
15. Singh PP (1994) Phys Rev Lett 72:2446
16. Singh PP (1994) Phys Rev B 49:4954
17. Paulus B, Rosciszewski K (2004) Chem Phys Lett 394:96
18. Gaston N, Paulus B, Rosciszewski K, Schwerdtfeger P, Stoll H (2006) Phys Rev B 74:094102
19. Gaston N, Schwerdtfeger P (2006) Phys Rev B 74:024105
20. Takemura K, Fujihisa H, Nakamoto Y, Nakano S, Ohishi Y (2007) J Phys Soc Jpn 76:023601
21. Schulte O, Holzapfel WB (1993) Phys Rev B 48:14009
22. Schulte O, Holzapfel WB (1996) Phys Rev B 53:569
23. Moriarty JA (1988) Phys Lett A 131:41
24. Jona F, Marcus PM (2007) J Phys Condens Matter 19:036103
25. Schwerdtfeger P, Gaston N, Krawczyk RP, Tonner R, Moyano GE (2006) Phys Rev B 73:0641121-19
26. Hermann A, Krawczyk RP, Lein M, Schwerdtfeger P, Hamilton IP, Stewart JJP (2007) Phys Rev A 76:013202
27. Jones RO, Gunnarsson O (1989) Rev Mod Phys 61:689
28. Kresse G, Furthmüller J (1996) Comp Math Sci 6:15
29. Hafner J (2008) J Comput Chem 29:2044
30. Moyano GE, Wesendrup R, Söhnel T, Schwerdtfeger P (2002) Phys Rev Lett 89:103401
31. Perdew JP, Burke K, Wang Y (1996) Phys Rev B 54:16533
32. Perdew JP (1991) In: Ziesche P, Eschrig H (eds) Electronic structure of solids 91. Akademie Verlag, Berlin, pp 11–20
33. Perdew JP, Burke K, Ernzerhof E (1996) Phys Rev Lett 77:3865
34. Perdew JP, Ruzsinszky A, Csonka GI, Vydrov OA, Scuseria GE, Constantin LA, Zhou X, Burke K (2008) Phys Rev Lett 100:136406
35. Wu X, Vargas MC, Nayak S, Lotrich V, Scoles G (2001) J Chem Phys 115:8748
36. Grimme S (2006) J Comp Chem 27:1787
37. Blöchl PE (1994) Phys Rev B 50:17953
38. Kresse G, Joubert D (1999) Phys Rev B 59:1758
39. Paier J, Marsman M, Hummer K, Kresse G, Gerber IC, Àngyán JG (2006) J Chem Phys 124:154709
40. Monkhorst HJ, Pack JD (1976) Phys Rev B 13:5188
41. Murnaghan FD (1944) Proc Nat Acad Sci (USA) 50:697
42. Barrett CS (1957) Acta Cryst 10:58
43. Paulus B (2006) Phys Rep 428:1
44. Harl J, Kresse G (2008) Phys Rev B 77:045136
45. Harl J, Kresse G (2009) Phys Rev Lett 103:056401
46. Janesko G, Henderson TM, Scuseria GE (2009) J Chem Phys 130:081105
47. Lide DR (ed) (1997) Handbook of chemistry and physics, 78th edn. CRC Press, London
48. Huntingdon HB (1958) Solid State Phys 7:282
49. Weaire D (1968) Philos Mag 18:213
50. Perdew JP, Chevary JA, Vosko SH, Jackson KA, Pederson MR, Singh DJ, Fiolhais C (1992) Phys Rev B 46:6671
51. Klement W Jr, Jayaraman A, Kennedy GC (1963) Phys Rev 131:1
52. Pahl E, Figgen D, Borschevsky A, Peterson KA, Schwerdtfeger P (2011) Theoret Chem Acc 129:651